<div align="right">**Paper CIT04-0546**</div>

THERMAL DISPERSION IN A POROUS MEDIUM MODELED AS AN ARRAY OF LONGITUDINALLY-DISPLACED ELLIPTIC RODS AS A FUNCTION OF THE SOLID-FLUID CONDUCTIVITY RATIO

Marcos Heinzelmann Junqueira Pedras
Instituto de Pesquisa e Desenvolvimento IP&D, UNIVAP
12244-000, São José dos Campos, SP, Brasil. E-mail: pedras@univap.br

Marcelo J.S. De-Lemos*
Departamento de Energia - IEME
Instituto Tecnológico de Aeronáutica - ITA
12228-900 - São José dos Campos - SP – Brasil, E-mail: delemos@mec.ita.br
* Corresponding author

Abstract. *Thermal dispersion in porous media is an import phenomenon in combustion and in steam injection systems for Enhanced Oil Recovery methods, among several others engineering applications. In this work, thermal dispersion tensors were calculated within an infinite porous medium formed by a spatially periodic array of longitudinally-displaced elliptic rods. Two different thermal conductivity ratios between the solid and fluid phases were used for analyzing their effect on the thermal dispersion tensor, following a systematic analysis of several porous media modeled by different unit-cell geometry. As such and for the sake of simplicity, just one unit-cell, together with periodic boundary conditions for mass and momentum equations, and Neumann and Dirichlet conditions for the energy equation, was used to represent such medium. The numerical methodology herein employed is based on the control-volume approach. Turbulence is assumed to exist within the fluid phase and a low Reynolds k-**e** closure is used to model it. The flow equations at the pore-scale were numerically solved using the SIMPLE method on a non-orthogonal boundary-fitted coordinate system. The integrated results were compared to the existing data presented in the literature.*

*Keywords: porous media, thermal dispersion, periodic boundary conditions, low Reynolds k-**e** model, macroscopic energy equation.*

1. Introduction

A systematic analysis on thermal dispersion in porous media has been carry out by Pedras *et al.* (2003b), Pedras *et al.* (2003c), Pedras *et al.* (2003d) and Pedras and de Lemos (2004) in order to contribute for the developing of a macroscopic transport equations based on the double-decomposition concept. (Pedras and de Lemos, 2001a; de Lemos and Pedras, 2001; Rocamora and de Lemos, 2000; Pedras and de Lemos, 2001b; Pedras and de Lemos, 2001c; Pedras and de Lemos, 2003a). This systematic development has numerically investigated the thermal dispersion in beds modeled as arrays of cylindrical rods (Pedras *et al.*, 2003b), longitudinally-displaced (Pedras *et al.*, 2003c; Pedras *et al.*, 2003d) and transversally-displaced (Pedras and de Lemos, 2004) elliptic rods. In all of these investigations the thermal conductivity ratios between the solid and fluid phases were the same and their results were compared with several different geometries. The long term objective of such research effort is to investigate the effect of the thermal conductivity ratio between the solid and fluid phases on dispersive transport in highly permeable media.

The investigations of thermal dispersion in porous media traditionally make use of the notion of Representative Elementary Volume, represented by Fig. 1, over which the transport equations are integrated (Hsu and Cheng, 1990; Kaviany, 1995; Ochoa-Tapia and Whitaker, 1997; Moyne, 1997; Quintard *et al.*, 1997; Kuwahara and Nakayama, 1998; Nakayama and Kuwahara, 1999). These models, based on the macroscopic point of view, lose details on the flow pattern inside the REV and, together with ad-hoc information, provide global flow properties such as average velocities and temperatures.

On the other hand, flow in porous media can also be analyzed by modeling the topology of the medium and resolving the flow equations at the pore-scale. This treatment reveals the flow structure at the pore-level an was used by Quintard *et al.* (1997), Kuwahara and Nakayama (1998), Nakayama and Kuwahara (1999) and Rocamora and de Lemos (2002) to determine the thermal dispersion tensors with periodic boundary conditions for mass, momentum and energy equations.

The aim of the present contribution is to present thermal dispersion coefficients obtained in a medium modeled as an infinity array of longitudinally-displaced elliptic rods with two different thermal conductivity ratios between the solid and fluid phases, $k_s/k_f = 2$ and $k_s/k_f = 10$. Where the results for $k_s/k_f = 2$ were already presented by Pedras *et al.* (2003c) whereas the results for $k_s/k_f = 10$ and the comparison between them will be presented in this work.
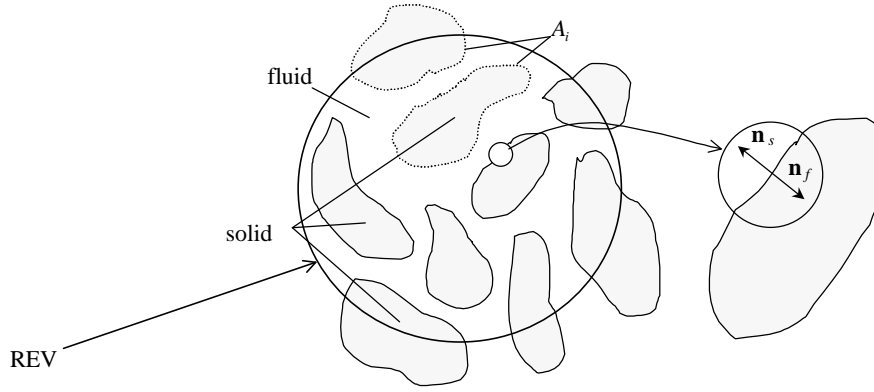
Figure 1.   Representative elementary volume (REV).

2. Microscopic Equations

The thermal dispersion modeling and the macroscopic and microscopic equations herein utilized can be found in Pedras *et al.* (2003b; 2003c and 2003d), however for the sake of comprehensiveness some of those equations will be presented once more.

The following microscopic transport equations describe the flow field and the heat transfer process within a porous medium, where barred quantities represent time-averaged components and primes indicate turbulent fluctuations:

Fluid Phase (incompressible fluid):

$$\nabla \cdot \overline{\mathbf{u}} = 0 \tag{1}$$

$$\boldsymbol{r}_f[\frac{\partial \overline{\mathbf{u}}}{\partial t} + \nabla \cdot (\overline{\mathbf{u}}\,\overline{\mathbf{u}})] = -\nabla \overline{p} + \nabla \cdot \{\boldsymbol{m}[\nabla \overline{\mathbf{u}} + (\nabla \overline{\mathbf{u}})^T] - \boldsymbol{r}_f \overline{\mathbf{u}'\mathbf{u}'}\} \tag{2}$$

$$\boldsymbol{r}_f c_{pf}[\frac{\partial \overline{T}_f}{\partial t} + \nabla \cdot (\overline{\mathbf{u}}\,\overline{T}_f)] = \nabla \cdot [k_f \nabla \overline{T}_f - \boldsymbol{r}_f c_{pf} \overline{\mathbf{u}'T'_f}] \tag{3}$$

$$\boldsymbol{r}_f[\frac{\partial k}{\partial t} + \nabla \cdot (\overline{\mathbf{u}}k)] = \nabla \cdot [(\boldsymbol{m} + \frac{\boldsymbol{m}_t}{\boldsymbol{s}_k})\nabla k] - \boldsymbol{r}_f \overline{\mathbf{u}'\mathbf{u}'}:\nabla \overline{\mathbf{u}} - \boldsymbol{r}_f \boldsymbol{e} \tag{4}$$

$$\boldsymbol{r}_f[\frac{\partial \boldsymbol{e}}{\partial t} + \nabla \cdot (\overline{\mathbf{u}}\boldsymbol{e})] = \nabla \cdot [(\boldsymbol{m} + \frac{\boldsymbol{m}_t}{\boldsymbol{s}_e})\nabla \boldsymbol{e}] + [C_1(-\boldsymbol{r}_f \overline{\mathbf{u}'\mathbf{u}'}:\nabla \overline{\mathbf{u}}) - C_2 f_2 \boldsymbol{r}_f \boldsymbol{e}]\frac{\boldsymbol{e}}{k} \tag{5}$$

$$-\boldsymbol{r}_f \overline{\mathbf{u}'\mathbf{u}'} = \boldsymbol{m}_t[\nabla \overline{\mathbf{u}} + (\nabla \overline{\mathbf{u}})^T] - \frac{2}{3}\boldsymbol{r}_f k\mathbf{I} \tag{6}$$

$$-\boldsymbol{r}_f c_{pf} \overline{\mathbf{u}'T'_f} = \boldsymbol{r}_f c_{pf} \frac{\boldsymbol{n}_t}{\boldsymbol{s}_t}\nabla \overline{T}_f \tag{7}$$

$$\boldsymbol{m}_t = \boldsymbol{r}_f \boldsymbol{n}_t = \boldsymbol{r}_f C_{\boldsymbol{m}} f_{\boldsymbol{m}} \frac{k^2}{\boldsymbol{e}} \tag{8}$$

Solid Phase:

$$\boldsymbol{r}_s c_{ps} \frac{\partial \overline{T}_s}{\partial t} = \nabla \cdot [k_s \nabla \overline{T}_s] \tag{9}$$

where $\mathbf{u}$ is the microscopic velocity, $\boldsymbol{r}_f$ and $\boldsymbol{r}_s$ the fluid and solid densities, p the thermodynamic pressure, $\boldsymbol{m}$ and $\boldsymbol{m}_t$ the dynamic and turbulent viscosities, T_f and T_s the fluid and solid temperatures, c_{pf} and c_{ps} the fluid and solid specific heat at constant pressure, k_f and k_s the fluid and solid thermal conductivities, k the turbulent kinetic energy and $\boldsymbol{e}$ the dissipation of k. In the equations $\boldsymbol{s}_k$, $\boldsymbol{s}_e$ and $\boldsymbol{s}_t$ are effective Prandtl numbers, C_1, C_2 and $C_{\boldsymbol{m}}$ are dimensionless constants and f_2 and $f_{\boldsymbol{m}}$ damping functions.

To account for turbulence the low Reynolds *k*-*e* closure was applied, utilizing the damping functions and model constants of Abe *et al.*, (1992).

For the unit-cell represented in Fig. (2) and with the assumption of macroscopic fully developed uni-dimensional flow, the boundary conditions are given as follow:

at the walls, $\overline{\mathbf{u}} = 0$; $\overline{T}_f = \overline{T}_s$; $\mathbf{n}_f \cdot (k_f \nabla \overline{T}_f) = -\mathbf{n}_s \cdot (k_s \nabla \overline{T}_s)$; $k = 0$ and $\boldsymbol{e} = \boldsymbol{n}\dfrac{\partial^2 k}{\partial n^2}$, $\qquad(10)$

on $x = 0$ and $x = H$ periodic boundaries (momentum equation),

$$\overline{u}\big|_{x=0} = \overline{u}\big|_{x=H} , \ \overline{v}\big|_{x=0} = \overline{v}\big|_{x=H} , \ k\big|_{x=0} = k\big|_{x=H} \ \text{and} \ \boldsymbol{e}\big|_{x=0} = \boldsymbol{e}\big|_{x=H} \qquad(11)$$

on $y = 0$ and $y = H$,

$$\frac{\partial \overline{u}}{\partial y} = \frac{\partial \overline{v}}{\partial y} = \frac{\partial k}{\partial y} = \frac{\partial \boldsymbol{e}}{\partial y} = 0 \qquad(12)$$

where n_f and n_s are the coordinates normal to the interface (Fig. 1) and u and v the components of $\mathbf{u}$.
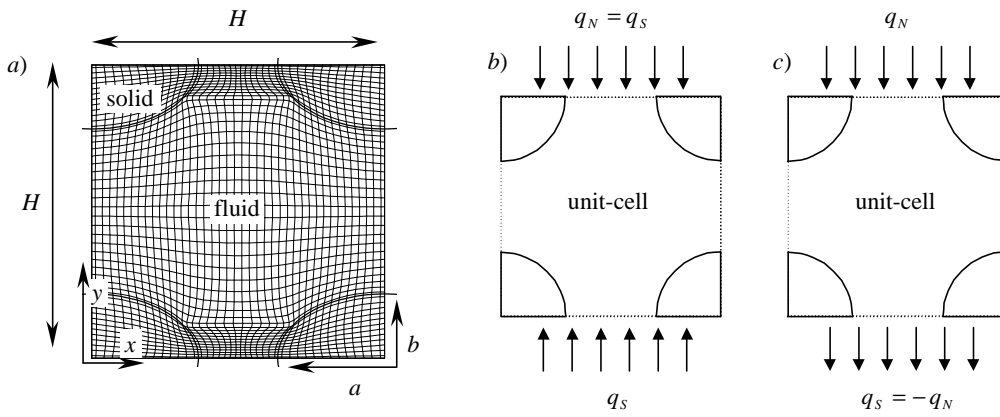
Figure 2. Unit-cell: *a*) elliptically generated grid ($a/b = 5/3$), *b*) and *c*) Neumann boundary conditions for the temperature $k_f \dfrac{\partial \overline{T}}{\partial y} = k_s \dfrac{\partial \overline{T}}{\partial y} = -q$.

The temperature boundary conditions will be presented in the next section.

3. Thermal Dispersion Modeling

The thermal dispersion modeling utilized in this work follow the same procedure of Pedras *et al.* (2003b; 2003c and 2003d). The macroscopic energy equation obtained by the volume averaging of the microscopic energy equations, Eqs. (3) and (9), over the REV, assuming local thermal equilibrium (*i.e.* $\langle \overline{T}_f \rangle^f = \langle \overline{T}_s \rangle^s = \langle \overline{T} \rangle$), was:

$$[\boldsymbol{f}_f \boldsymbol{r}_f c_{pf} + \boldsymbol{f}_s \boldsymbol{r}_s c_{ps}]\frac{\partial \langle \overline{T} \rangle}{\partial t} + \boldsymbol{r}_f c_{pf} \nabla \cdot (\langle \overline{\mathbf{u}} \rangle \langle \overline{T} \rangle) = \nabla \cdot \mathbf{K}_{eff} \cdot \nabla \langle \overline{T} \rangle \qquad(13)$$

where $\langle \overline{T} \rangle$ is the volume average of the time averaged temperature, $\langle \overline{T}_b \rangle^b$ the intrinsic average of the time averaged temperature in the $\boldsymbol{b}$ phase, $\boldsymbol{f}_f$ the volume fraction of fluid and $\boldsymbol{f}_s = 1 - \boldsymbol{f}_f$ the volume fraction of solid. The effective conductivity, $\mathbf{K}_{eff}$, the tortuosity tensor, $\mathbf{K}_{tor}$, and the dispersion tensor, $\mathbf{K}_{dis}$, are defined as:

$$\mathbf{K}_{eff} = (\boldsymbol{f}_f \frac{\boldsymbol{r}_f c_{pf} \boldsymbol{n}_{t_f}}{\boldsymbol{s}_t} + \boldsymbol{f}_f k_f + \boldsymbol{f}_s k_s)\mathbf{I} + \mathbf{K}_{tor} + \mathbf{K}_{dis} \qquad(14)$$

$$\mathbf{K}_{tor} \cdot \nabla \langle \overline{T} \rangle = \frac{(k_f - k_s)}{\Delta V} \int_{A_i} \mathbf{n}_f \, {}^i\overline{T}_f \, dS \qquad(15)$$

$$\mathbf{K}_{dis} \cdot \nabla \langle \overline{T} \rangle = -\boldsymbol{r}_f c_{pf} \boldsymbol{f}_f \langle {}^i\overline{\mathbf{u}} \, {}^i\overline{T}_f \rangle^f = -\frac{\boldsymbol{r}_f c_{pf}}{\Delta V} \int_{\Delta V_f} {}^i\overline{\mathbf{u}} \, {}^i\overline{T}_f \, dV \qquad(16)$$

where $^i\boldsymbol{j}$ is the space deviation of $\boldsymbol{j}$.

If the gradient of the average temperature is in the same direction of the macroscopic flow or transverse to it, only diagonal components of $\mathbf{K}_{dis}$ remain non-zero components. In these conditions, Eq. (16) renders, respectively, for the diagonal components of $\mathbf{K}_{dis}$,

$$(K_{dis})_{xx} = -\frac{\dfrac{\boldsymbol{r}_f\,c_{pf}}{\Delta V}}{\dfrac{\Delta\langle\overline{T}\rangle_x}{H}}\int\limits_{\Delta V_f}{}^i\overline{u}\;{}^i\overline{T}_f\,dV \tag{17}$$

$$(K_{dis})_{yy} = -\frac{\dfrac{\boldsymbol{r}_f\,c_{pf}}{\Delta V}}{\dfrac{\Delta\langle\overline{T}\rangle_y}{H}}\int\limits_{\Delta V_f}{}^i\overline{v}\;{}^i\overline{T}_f\,dV \tag{18}$$

In Eqs. (17) and (18) the gradients $\Delta\langle\overline{T}\rangle_x$ and $\Delta\langle\overline{T}\rangle_y$ can be calculated in two ways. The first one is using the Neumann boundary conditions sketched, respectively, in Figs. (2b and 2c). In this case $\Delta\langle\overline{T}\rangle_x$ and $\Delta\langle\overline{T}\rangle_y$ are given as,

$$\Delta\langle\overline{T}\rangle_x = \frac{1}{H}\int\limits_{y=0}^{y=H}[\overline{T}_{x=H}-\overline{T}_{x=0}]dy \quad\text{and}\quad \Delta\langle\overline{T}\rangle_y = \frac{1}{H}\int\limits_{x=0}^{x=H}[\overline{T}_{y=H}-\overline{T}_{y=0}]dx \tag{19}$$

The second way is using Dirichlet boundary conditions (Kuwahara and Nakayama, 1998 and Rocamora and de Lemos, 2002) for the energy equation,

$$\overline{T}_{x=0}=\overline{T}_{x=H}-\Delta\langle\overline{T}\rangle_x \;\text{ and }\; \overline{T}_{y=0}=\overline{T}_{y=H} \tag{20}$$

for the $(K_{dis})_{xx}$ calculation, and,

$$\overline{T}_{x=0}=\overline{T}_{x=H} \;\text{ and }\; \overline{T}_{y=0}=\overline{T}_{y=H}-\Delta\langle\overline{T}\rangle_y \tag{21}$$

for the $(K_{dis})_{yy}$ calculation. In this case $\Delta\langle\overline{T}\rangle_x$ and $\Delta\langle\overline{T}\rangle_y$ are constants.

4. Numerical Model

The transport equations at the pore-scale were numerically solved using the SIMPLE method on a non-orthogonal boundary-fitted coordinate system. The equations were discretized using the finite volume procedure of Patankar (1980). The solving process starts with the solution of the two momentum equations and the velocity fields is adjusted in order to satisfy the continuity principle. This adjustment is attained by solving the pressure correction equation. After that, the turbulence model and the energy equations are relaxed to update the the k, $\boldsymbol{e}$ and temperature fields. Details on the numerical discretization can be found in Pedras and de Lemos (2001b).

As in the former works (Pedras *et al.*, 2003b; 2003c; 2003d and Pedras and de Lemos, 2004), just one unit-cell, together with periodic boundary conditions for mass and momentum equations, and Neumann and Dirichlet conditions for the energy equation, was used to represent the porous medium. For a fixed flow and the Neumann temperature conditions (Fig. 2b, c) the thermal dispersion tensors were calculated after a sequence of converged loops on the same run. This sequence of loops is necessary for the temperature field development, whereas for the velocity field this is not necessary because of the periodic boundary conditions used. The temperature development was carried out using the outlet temperature of a loop as the inlet temperature for the next loop. This procedure is repeated until we have no change in the temperature deviation field.

In the low Re model, the node adjacent to the wall requires that $u_t n/\boldsymbol{n}\leq 1$. To accomplish this requirement, the grid needs points close to the wall leading to computational meshes of 40×54 nodes. A highly non-uniform grid arrangement was employed with concentration of nodes close to the wall. Values for $(K_{dis})_{xx}$ and $(K_{dis})_{yy}$ were obtained varying the $\mathrm{Pe}_H = |\langle\overline{\mathbf{u}}\rangle|\,H/\boldsymbol{a}_f$ from 10^0 to 4.10^3 and the $\boldsymbol{f}_f = 1 - ab\pi/H^2$, from 0.60 to 0.90.

5. Results and Discussion

As in the work of Pedras *et al.* (2003c) a total of twenty seven runs were carried out being twenty three for laminar flow and four for turbulent flow with the low Re model theory. In all runs it was used for the fluid phase a Prandtl number of 0.72 and a thermal conductivity ratio between the solid and fluid phase of $k_s/k_f = 10$.

The temperature fields calculated with the temperature boundary conditions sketched in Fig. (2b) are presented in the Fig. (3), while the temperature fields calculated with the same flow rate but using the temperature boundary conditions Eq. (20) are presented in Fig. (4). In both figures, the gradients of the average temperature are in the same direction of the macroscopic flow. As will be shown further, in spite of the differences in the temperature fields obtained principally in the solid phase, the values of the longitudinal component of $\mathbf{K}_{dis}$ were very similar. This behavior can be explained with the own definition of the $\mathbf{K}_{dis}$ (Eq. 16), *i.e.*, the determination of $\mathbf{K}_{dis}$ is driven by the deviation fields of velocity and temperature within the fluid phase and looking closely in the fluid phase the temperature fields, for the same flow rate, resemble fairly each other.
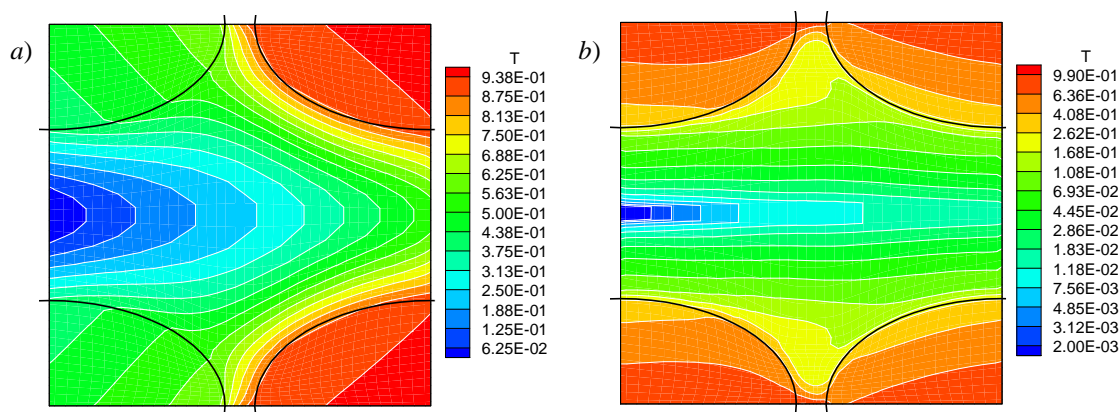
Figure 3.   Temperature fields calculated with the temperature boundary conditions sketched in Fig. (2b) and $\mathbf{f}_f = 0.60$: *a*) $\mathrm{Pe}_H = 10$, and *b*) $\mathrm{Pe}_H = 4 \times 10^3$.
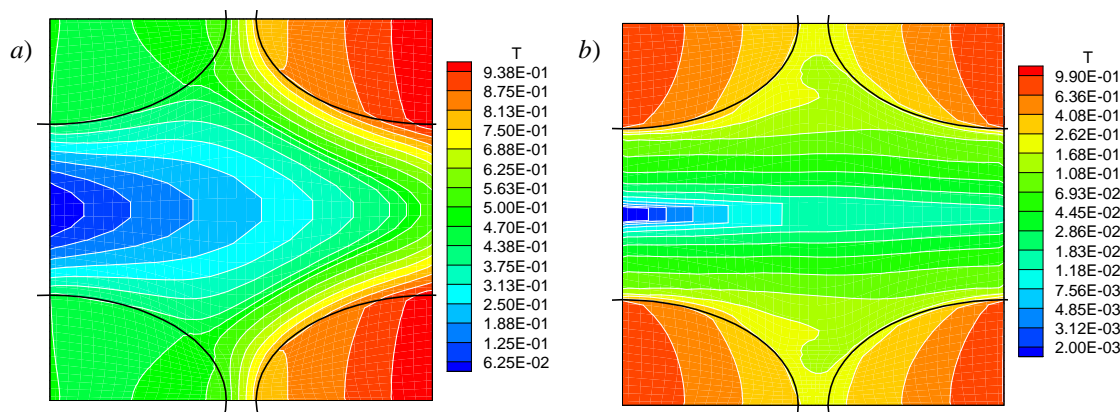
Figure 4.   Temperature fields calculated with the temperature boundary conditions, Eq. (20), and $\mathbf{f}_f = 0.60$: *a*) $\mathrm{Pe}_H = 10$; and *b*) $\mathrm{Pe}_H = 4 \times 10^3$.

The temperature fields calculated with the boundary conditions sketched in Fig. (2c) and with Eq. (21) are presented, respectively, in the Figs. (5) and (6), in which the gradients of the average temperature are in the transverse direction to the macroscopic flow. For the same flow rate the temperature fields resemble fairly each other in the whole field and, consequently (as discussed before), the transverse component of $\mathbf{K}_{dis}$ were very similar in both boundary conditions. Furthermore, Figs. (5b) and (6b) show the same behavior of Figs. (3b) and (4b), *i.e.*, as the flow rate increases the fluid temperature becomes more uniform due to the mixing produced in the flow.
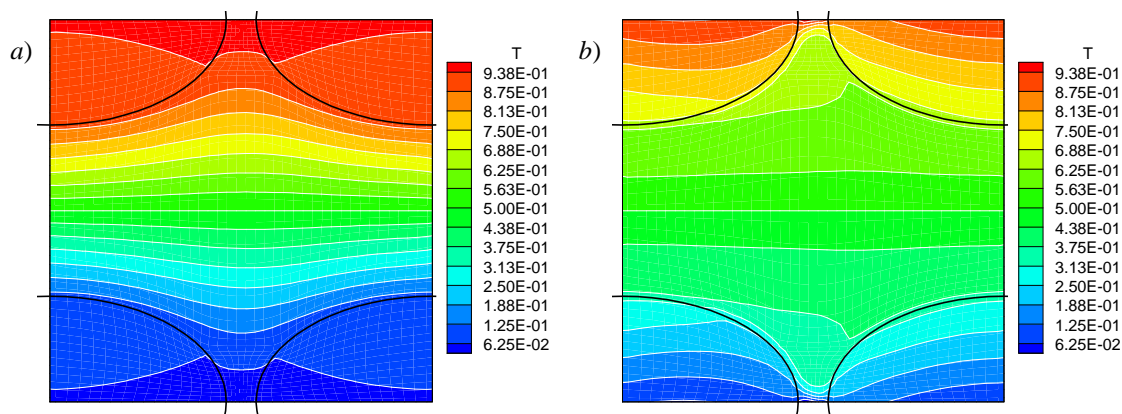
Figure 5. Temperature fields calculated with the temperature boundary conditions sketched in Fig. (2c) and $f_f = 0.60$: *a*) $Pe_H = 10$, and *b*) $Pe_H = 4 \times 10^3$.
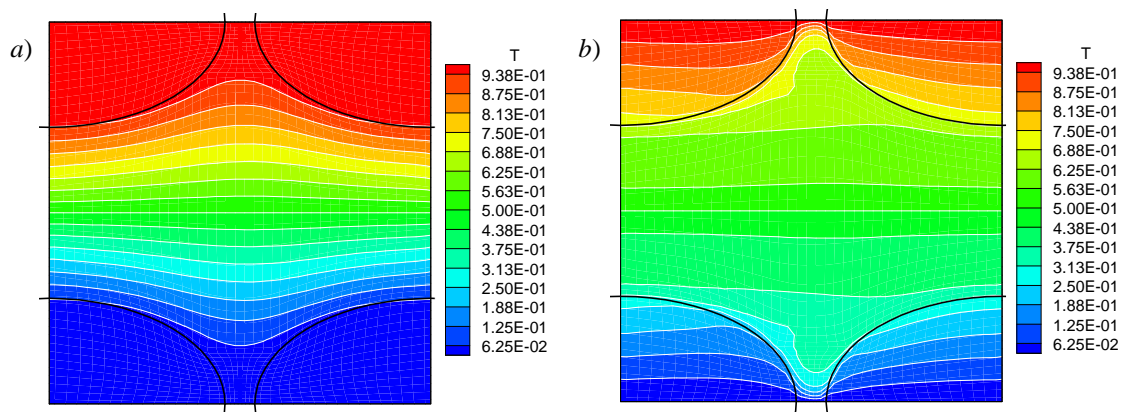
Figure 6. Temperature fields calculated with the temperature boundary conditions, Eq. (21), and $f_f = 0.60$: *a*) $Pe_H = 10$, and *b*) $Pe_H = 4 \times 10^3$.

Figure (7) shows the longitudinal component of the thermal dispersion tensor as a function of the Peclet number and different porosities. The results shows good agreement when compared with the data of Kuwahara and Nakayama (1998) and Rocamora and de Lemos (2002), for square and cylindrical rods, respectively. As mentioned before, the use of different boundary conditions (Fig. 2b and Eq. 20) yields very little differences in the longitudinal component of $\mathbf{K}_{dis}$. Its overall dependence on the Peclet number was $(K_{dis})_{xx}/k_f = 3.45 \times 10^{-2} Pe_H^{1.65}$, showing the usual behavior of $\sim Pe_H^{\,n}$ as expected.

The comparison between the longitudinal components calculated with $k_s/k_f = 2$ (Pedras *et al.*, 2003c, where $(K_{dis})_{xx}/k_f$ was $3.52 \times 10^{-2} Pe_H^{1.65}$) and with $k_s/k_f = 10$ is shown in Fig (8). The results shown that the longitudinal component had little variance for this two conductivity ratios, moreover, Fig (7a) also shows that for different morphologies (longitudinal-displaced elliptic, square and cylindrical rods) the variances were also very little. A possible explanation for this fact is that in all cases were used a Prandtl number of 0.72 and, then, for a same Peclet number we will have a same convected temperature in the direction of the main flow.
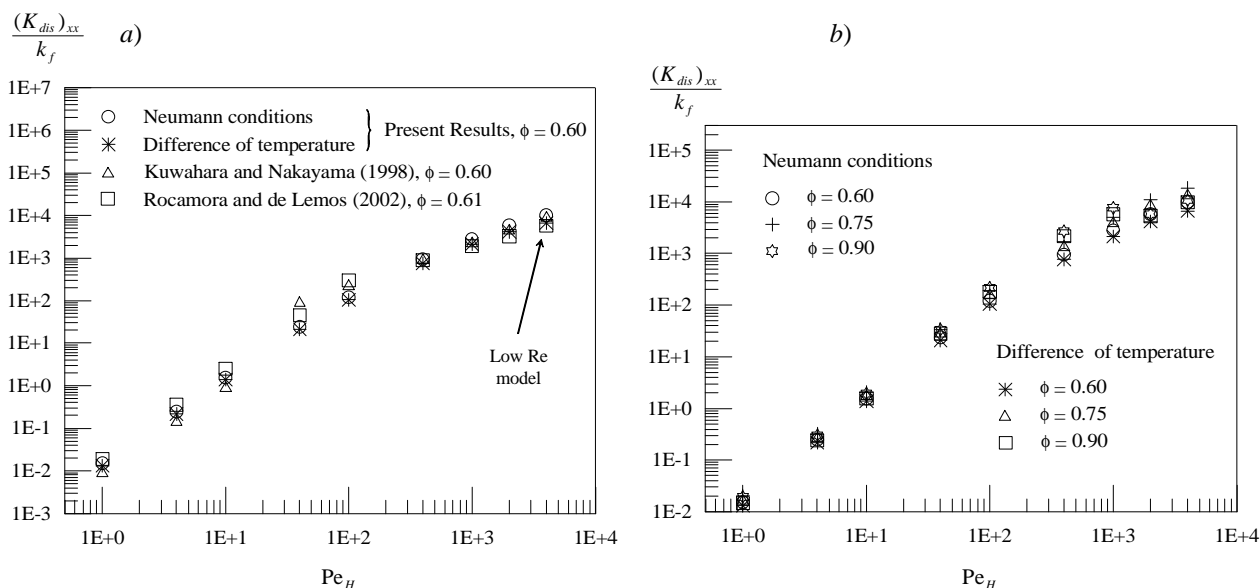
Figure 7.   Longitudinal thermal dispersion: *a*) $f_f = 0.60$ and *b*) overall results.
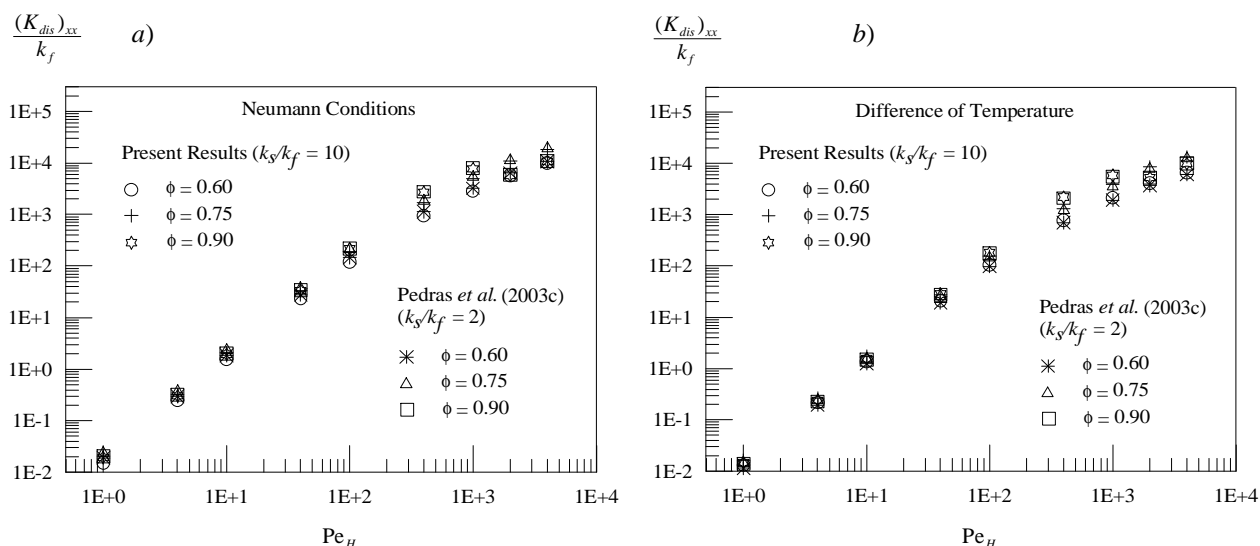
Figure 8.   Longitudinal thermal dispersion comparing between $k_s/k_f = 2$ and $k_s/k_f = 10$: *a*) Neumann boundary conditions, Fig. (2b), and *b*) temperature boundary conditions, Eq. (20).

In the same way, the transverse component of the thermal dispersion is shown in Fig (9). As already mentioned, the use of different boundary conditions (Fig. 2c and Eq.21) yields very little differences in the transverse component of $\mathbf{K}_{dis}$. On the other hand, different morphologies (longitudinal-displaced elliptic, square and cylindrical rods) yield great differences in its values (Fig. 9a). The results of Kuwahara and Nakayama (1998), for square rods, were greater than that from Rocamora and de Lemos (2002), for cylindrical rods, which were greater than the present results. The overall dependence of the transverse component on the Peclet number was $(K_{dis})_{yy}/k_f = 1.55 \times 10^{-4} \mathrm{Pe}_H^{0.94}$.

The Fig. (10) shows the comparison between the transverse components calculated with $k_s/k_f = 2$ (Pedras *et al.*, 2003c, where $(K_{dis})_{yy}/k_f$ was $= 2.29 \times 10^{-4} \mathrm{Pe}_H^{0.88}$) and with $k_s/k_f = 10$. The comparison shows that the transverse component was more sensible to the variation of the conductivity ratio than the longitudinal component, principally for a Peclet number of about 10^2. In this range of Peclet number we had a little recirculating zone behind the rods (between the two in-line rods in the south and north region of the unit-cell) and for $k_s/k_f = 10$ the transverse components were very little (some times $(K_{dis})_{yy}/k_f$ were less than 10^{-5}). On the other hand, for $k_s/k_f = 2$ this not occur, a possible explanation for this occurrence is in the temperature gradients obtained in each case. For $k_s/k_f = 2$ the temperature gradient in the recirculating zones was so greater than that obtained for $k_s/k_f = 10$ (almost zero as in the Fig. 6a, blue and red zones). This almost zero temperature gradient along with the recirculating zone chokes the transverse

dispersion, *i.e.*, the central region of the flow, that is not recirculating, works as a developed flow in two parallel plates, which, from Eq. (18), has a transverse dispersion equal to zero.
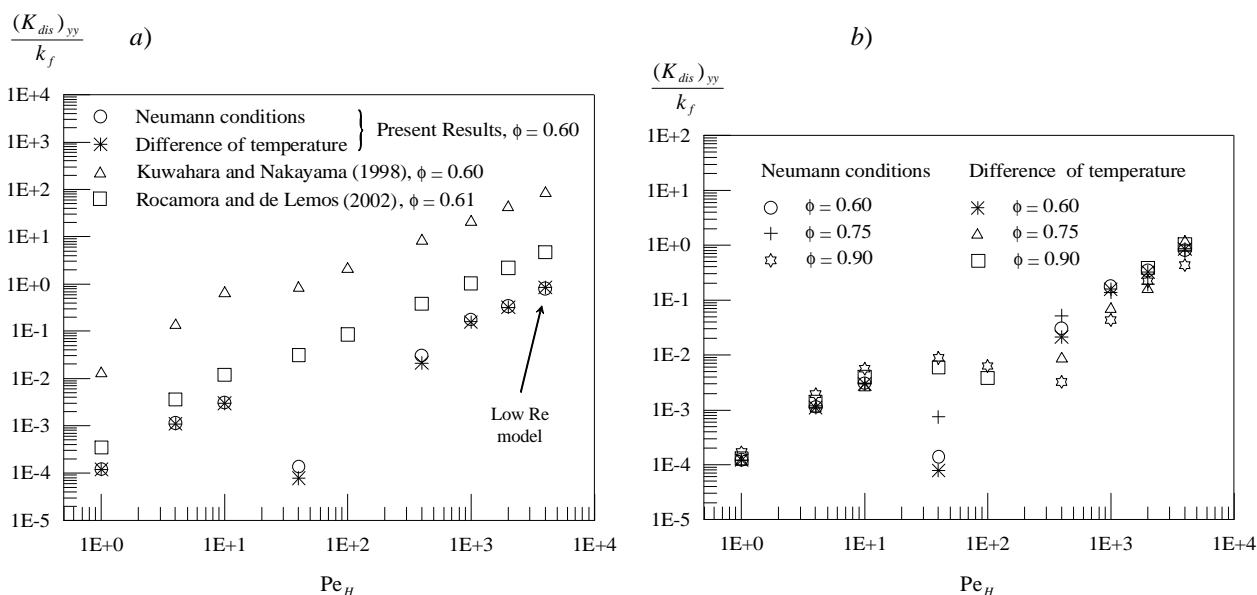
Figure 9.   Transverse thermal dispersion: *a)* $\boldsymbol{f}_f = 0.60$ and *b)* over all results.
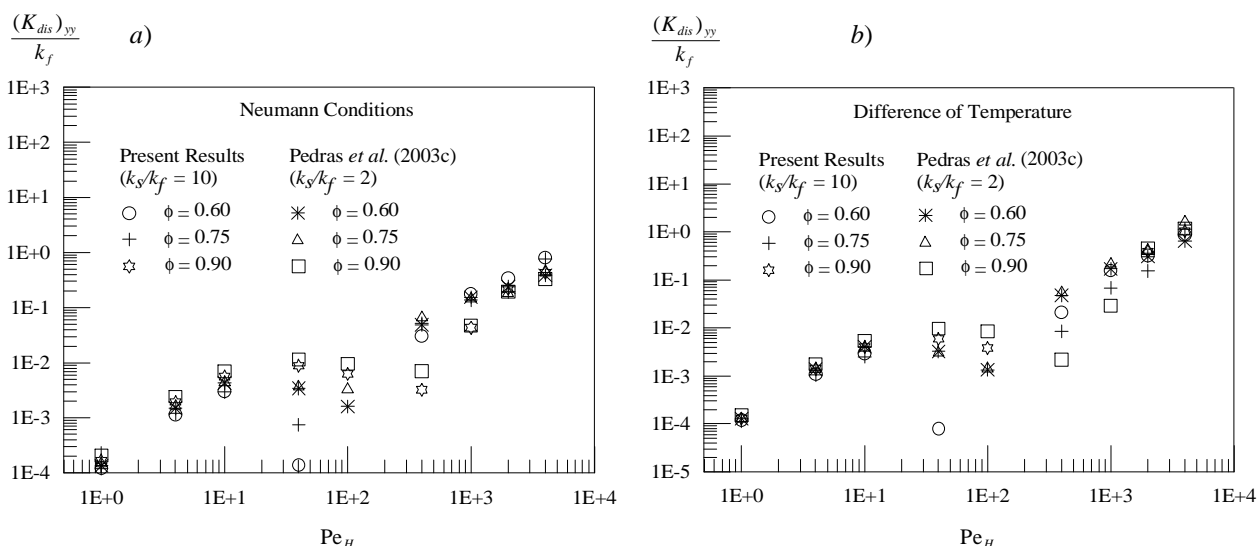
Figure 10.   Transverse thermal dispersion comparing between $k_s/k_f = 2$ and $k_s/k_f = 10$: *a)* Neumann boundary conditions, Fig. (2c), and *b)* temperature boundary conditions, Eq. (21).

6.   Conclusions

Results of thermal dispersion components calculated for a periodic porous medium modeled as an infinite array of longitudinally-displaced elliptic rods with a thermal conductivity ratio between the solid and fluid phase of 10 were presented. For the sake of simplicity, this porous medium was represented by a unit-cell with Neumann and Dirichlet boundary conditions for the energy equation and periodic boundary conditions for mass and momentum equations. Finally the results were compared with data found in the literature for the same porous medium but with a thermal conductivity ratio of 2 and for porous media with different geometries.

7.   Acknowledgements

8. References

Abe, K., Nagano, Y., and Kondoh, T., 1992, "An Improved k-ε Model for Prediction of Turbulent Flows with Separation and Reattachment", Trans. JSME, Ser. B, vol. 58, pp. 3003-3010.

de Lemos, M.J.S. and Pedras, M.H.J., 2001, "Recent Mathematical Models for Turbulent Flow in Saturated Rigid Porous Media", ASME Journal of Fluids Engineering, vol. 123 (4), pp. 935-940.

Hsu, C. T. and Cheng, P., 1990, "Thermal Dispersion in a Porous Medium", Int. J. Heat Mass Transfer, vol. 33, pp. 1587-1597.

Kaviany, M., 1995, "Principles of Heat Transfer in Porous Media", 2nd edn. Springer, New York.

Kuwahara, F. and Nakayama, A., 1998, "Numerical Modeling of Non-Darcy Convective Flow in Porous Medium", Proc. of 11th IHTC (Kyongju, Korea), vol. 4, pp. 411-416.

Moyne, C., 1997, "Two-Equation Model for a Diffusive Process in Porous Media Using the Volume Averaging Method with an Unsteady-State Closure", Adv. Water Resour., vol. 20 (2-3), pp. 63-76.

Nakayama, A. and Kuwahara, F., 1999, "A Macroscopic Turbulence Model for Flow in a Porous Medium", ASME Journal of Fluids Engineering, vol. 121, pp. 427-433.

Ochoa-Tapia, J. A. and Whitaker, S., 1997, "Heat Transfer at the Boundary Between a Porous Medium and a Homogeneous Fluid", Int. J. Heat Mass Transfer, vol. 40 (11), pp. 2691-2707.

Patankar, S. V., 1980, "Numerical Heat Transfer and Fluid Flow", Hemisphere, New York.

Pedras, M.H.J. and de Lemos, M.J.S., 2001a, "Macroscopic Turbulence Modeling for Incompressible Flow Through Undeformable Porous Media", Int. J. Heat Mass Transfer, vol. 44 (6), pp. 1081-1093.

Pedras, M.H.J. and de Lemos, M.J.S., 2001b, "Simulation of Turbulent Flow in Porous Media Using a Spatially Periodic Array and a Low Re Two-Equation Closure", Numer. Heat Transfer, Part A-Appl, vol. 39 (1), pp. 35-59.

Pedras, M.H.J. and de Lemos, M.J.S., 2001c, "On Mathematical Description and Simulation of Turbulent Flow in a Porous Medium Formed by an Array of Elliptic Rods", ASME Journal of Fluids Engineering, vol. 123 (4), pp. 941-947.

Pedras, M.H.J. and de Lemos, M.J.S., 2003a, "Computation of Turbulent Flow in Porous Media Using a Low Reynolds k-e Model and an Infinite Array of Transversally Displaced Elliptic Rods", Numer. Heat Transfer; Part A-Appl. vol. 43, n. 6, pp. 585-602.

Pedras, M.H.J., Rocamora, F.D. and de Lemos, M.J.S., 2003b, "Simulation of Turbulent Thermal Dispersion in Porous Media Using a Periodic Cell with Prescribed Heat Flux at the Boundaries", Proc. of 3rd Int. Conf.. Computational Heat and Mass Trans., May 26-30, Banff, Canada.

Pedras, M.H.J., Rocamora Jr, F.D. and de Lemos, M.J.S., 2003c, "Turbulent Dispersion in a Porous Media Modeled as an Infinite Array of Longitudinally-Displaced Elliptic Rods", Proc. of the COBEM2003 17th Int. Cong. of Mechanical Engineering, November 10-14, São Paulo, Brazil.

Pedras, M.H.J., Rocamora Jr, F.D. and de Lemos, M.J.S., 2003d, "Thermal Dispersion in a Porous Medium Modeled as an Array of Elliptic Rods, *J. Heat Transfer* (submitted).

Pedras, M.H.J. and de Lemos, M.J.S., 2004, "Turbulent Dispersion in Porous Media Modeled as an Infinite Array of Transversally-Displaced Elliptic Rods", Proc. of the ICAPM 2004 2nd Int. Conf. on Applications of Porous Media, May 24-27, Evora, Portugal.

Quintard, M., Kaviany, M. and Whitaker, S., 1997, "Two-Medium Treatment of Heat Transfer in Porous Media: Numerical Results for Effective Proprieties", Adv. Water Resour., vol. 20 (2-3), pp. 77-94.

Rocamora, F.D. and de Lemos, M.J.S., 2000, "Analysis of Convective Heat Transfer for Turbulent Flow in Saturated Porous Media", Intern. Comm. Heat and Mass Transfer, vol. 27 (6), pp. 825-834.

Rocamora, F.D., de Lemos M.J.S. 2002, "Numerical Determination Of The Thermal Dispersion Tensor In An Infinite Porous Medium", Numerical Heat Transfer (submitted).

9. Copyright Notice